RESEARCH ARTICLE

Obtaining bio-oil and activated carbon from waste pomegranate peels by pyrolysis

Oğuzhan Alagöz[1] · Nazan Yılmaz[1] · Meltem Dilek[1]

Abstract

This study aims to produce beneficial products with pomegranate peel waste through pyrolysis. For this purpose, the usability of the liquid product as a biofuel and the solid product as an adsorbent for dye removal was investigated. To characterize the bio-oil and biochar produced under the best pyrolysis conditions, Fourier transforms infrared spectroscopy (FT-IR), Gas chromatography-mass spectrometry (GC–MS), calorific value, Brunauer–Emmett–Teller (BET), and Scanning electron microscopy (SEM) analyses were conducted. When we examine the FT-IR spectrum of the bio-oil, the presence of phenol, alcohol, ketone, and aldehyde groups is seen in the structure. The GC–MS analysis demonstrated that phenol content was 27.9%, aldehyde content was 19%, acid compound content was 18.28%, ketone content was 8.7%, and aromatic compound content was 8.4%. The lower calorific value of bio-oil was determined as 27.33 MJ/kg. It was observed that activated carbon produced from biochar at a 3:1 KOH/biochar impregnation ratio and a carbonization temperature of 800 °C exhibited the highest surface area (1307 m^2/g). In adsorption analysis, it was observed that the adsorption efficiency was higher at pH 9 and 35 °C and with 150 ppm initial concentration. Langmuir and Freundlich adsorption isotherms were determined, and the high R^2 (0.99) was consistent with the Langmuir methylene blue (MB) adsorption model.

Keywords Renewable energy · Biomass thermal conversion · Biofuel · Activated char · Methylene blue · Waste biomass

Introduction

Energy resources are essential and indispensable for sustaining industrial and social life (Owusu and Asumadu-Sarkodie 2016). Global energy demand has increased rapidly due to population growth and economic developments. Approximately 85% of the daily global energy demand is produced from fossil fuels (Varma and Mondal 2016). The amount of global fossil CO_2 emissions per capita (4.81 t CO_2/person), resulting from the consumption of traditional fossil fuels such as coal, oil, and natural gas, increased by about 13% between 1990 and 2021 (Crippa et al. 2022). Therefore, it is essential to search for alternative energy sources. Biofuel is an alternative climate and environment-friendly source that reduces CO_2 gas emissions (Siddiqui et al. 2019).

Biomass is the only energy source among renewable energy sources that could produce solid, liquid, and gaseous products (Bridgwater and Peacocke 2000). The production entails two main conversion processes, thermochemical and biochemical, to obtain high-added-value biomass products. Thermochemical biomass conversion entails gasification, pyrolysis, hydrothermal liquefaction, and combustion (Jha et al. 2022). Pyrolysis is an efficient thermochemical conversion method for transforming biomass into biofuel. The rapid progress of studies on pyrolysis is promising for commercializing the process (Varma and Mondal 2016). In pyrolysis, organic materials in the biomass are heated in an oxygen-free environment to obtain liquid products (bio-oil, vapors that can be condensed at cooling temperatures), carbon-rich solid residues (char), and gaseous products (non-condensable synthetic gases) (Hassen-Trabelsi et al. 2014). The distribution of pyrolysis of biomass products depends on the pyrolysis parameters, such as process temperature, heating rate, reaction atmosphere (N_2, H_2, or H_2O (steam)), and reactor type (Jha et al. 2022). Biochar produced with

---

✉ Nazan Yılmaz
  nazanyilmaz@aku.edu.tr

[1] Department of Chemical Engineering, Faculty of Engineering, Afyon Kocatepe University, 03200 Afyonkarahisar, Turkey

pyrolysis can be used as a fuel (Ali et al. 2022), activated carbon (Zhong et al. 2023), or fertilizer due to its porous structure, surface area, and N, P, and K content. Bio-oil could be converted into high-value-added products and specialty chemicals as an energy source since it includes aromatic, aliphatic, naphthenic hydrocarbons, and oxygenated compounds. On the other hand, pyrolysis gas can be used to produce natural gas and synthesize certain chemical compounds since it includes CO, H_2, CO_2, CH_4, and other light hydrocarbons (Moralı and Şensöz 2015).

Pomegranate peels are one of the biomass raw materials. The pomegranate plant (*Punica granatum L.*) is grown mainly in Turkey's Mediterranean and Aegean regions (Ateş et al. 2019). Turkey's pomegranate production was approximately 600,000 tons in 2022 (Dilmen et al. 2022). In addition to being consumed as pomegranate fruit, products such as pomegranate syrup, juice, jam, and canned are produced from the plant. Pomegranate peel is an industrial by-product (İçyer 2012). Studies have been conducted on the pyrolysis of waste pomegranate seeds, pulp, and peel (Saadi et al. 2019; Kar 2018; Uçar and Karagöz 2009; Pehlivan and Özbay 2018; Ateş et al. 2019; Siddiqui et al. 2019).

This study aimed to investigate the transformation of pomegranate peel, a waste product available in large quantities, into more beneficial products via pyrolysis. Waste pomegranate peel was pyrolyzed in a fixed-bed reactor. The best pyrolysis conditions were determined by the pyrolysis of waste pomegranate peel in two particle sizes at different pyrolysis temperatures and heating rates. FT-IR, calorific value, and GC–MS analyses were conducted to characterize the liquid product (bio-oil) under the best pyrolysis conditions. To ensure that the solid pyrolysis product (biochar) could be used as an adsorbent dye removal from wastewater, activated carbon was produced with KOH activation. Activated carbon was characterized with SEM and BET analysis, and usability in dye removal was investigated.

Materials and methods

Materials

In the study, pomegranate peels, which were separated as waste after the production of pomegranate syrup by the local people in Antalya, were used as biomass raw material. The particle size of the pomegranate peel was reduced by using an industrial rounder. The reduced pomegranate peels were dried at room temperature and then in an oven at 105 °C for 6 h. The particle size of the dried pomegranate peel was determined with a vibrating sieve. Thus, pomegranate peel particles were separated into two sizes: 1.0–1.6 mm and 1.6–2.1 mm. Before pyrolysis, preliminary analyses were conducted to determine moisture, ash, volatile matter, oil,

cellulose, and lignin content. The moisture content was determined by a moisture analyzer (OHAUS) after samples were heated to 105 °C (ASTM D4442-16). The volatile matter and ash content were analyzed using ASTM D1102-84 and ASTM E872-82 methods. The amounts of lignin, cellulose, and hemicellulose in the pomegranate peel were determined according to ASTM D 1106–96, TS324, and ASTM D 1104–56, respectively. TGA/DTA (Thermogravimetric analysis/ Differential thermal analysis) of biomass was conducted to investigate the temperature range for effective pyrolysis. A Netzsch STA 449 F3 Jupiter model instrument was used for this analysis. The curve was obtained at a heating rate of 20 °C min^{-1} between 20 and 800 °C.

Methods

Pyrolysis

The pyrolysis of waste pomegranate peel was conducted with a stainless-steel fixed bed slow pyrolysis reactor. The heating was provided by a PID control element. It included an N_2 gas inlet and a condenser for condensation of the effluent gases.

Pyrolysis of the waste pomegranate peels in two particle sizes (1.0–1.6 mm and 1.6–2.1 mm) was conducted at four pyrolysis temperatures (400 °C, − 450 °C, − 500 °C, and 550 °C), 10 °C/min and 18 °C heating rates, and with a 1 L/min N_2 flow rate. Fifty grams of pomegranate peel was added to the reactor, and the pyrolysis temperature and heating rate were adjusted. The reactor reached and was kept at the target temperature for 20 min. Then, the reactor was cooled to room temperature. The solid product (biochar) in the reactor was carefully removed and weighed. The liquid product (bio-oil) was transferred into the container, and the condenser residue was washed with dichloromethane. The liquid product was taken into the separating funnel, the water and organic phases were separated, and the water content was weighed. The dichloromethane in the liquid product was separated with an evaporator, and the final liquid product was weighed. The gaseous product was determined with total mass balance. Pyrolysis experiments were repeated twice for all parameters. After the pyrolysis, bio-oil, biochar, and gas product yields were calculated.

Characterization

As a result of the pyrolysis studies, the best pyrolysis conditions where the highest liquid product (bio-oil) yield was obtained were determined. The bio-oil obtained under these conditions was characterized by GC–MS, FT-IR, and calorific value analyses. At the same time, the biochar obtained under the best pyrolysis conditions was activated, and the activated carbon was characterized by SEM ((scanning

electron microscope) and BET (Brunauer, Emmet, and Teller) analyses. The FT-IR spectrum of the bio-oil was recorded by preparing a KBr pellet with a Perkin Elmer 1605 FT-IR spectrometer. The compounds of the bio-oil were determined with a Shimadzu GC–MS/QP2020 instrument. GC–MS analysis was determined under the conditions presented in Table 1. SEM analysis was performed using the LEO 1430 VP model device. BET analysis was performed using Micromeritics brand Gemini VII 2390t model device.

Activated carbon production and adsorption

Biochar obtained from pyrolysis was activated, and its adsorbent properties were investigated for dye removal from wastewater. Activated carbon was produced from biochar with the chemical activation method and KOH. It was stored in solutions prepared with four impregnation rates (05:1, 1:1, 2:1, 3:1 KOH/biochar) for 24 h. Then, it was dried in an oven at 100 °C for 3 days to initiate carbonization. Carbonization was conducted at a heating rate of 10 °C/min and four different temperatures (500 °C, 600 °C, 700 °C, and 800 °C) for 60 min. After carbonization, the activated carbon with the highest surface area was determined and used for the adsorption of methylene blue (MB) dye. Several techniques have recently been used to remove dye pollutants from wastewater. Alternatively, adsorption has been considered one of the most available approaches to removing the dye in wastewater due to the advantages of lost cost, environmental friendliness, and highly effective and convenient operation (Cui et al. 2023). The effects of temperature, initial concentration, and pH on the adsorption were investigated. Adsorption tests were conducted with 0.1-g activated carbon and 100-mL methylene blue solution with an initial 100–150 ppm concentration. The absorbance of the methylene blue solution samples obtained at certain time intervals was measured at a wavelength of 664 nm with an ultraviolet–visible (UV–VIS) spectrophotometer, and concentrations were determined with a calibration chart. The adsorbed matter, the adsorption capacity of the adsorbent (q_e (mg/g)), and the percentage of methylene blue adsorbed (%MB) were calculated with the following equations:

$$qe = \frac{(Co - Ce)V}{W} \tag{1}$$

$$\%MB = \frac{Co - Ce}{Co} \times 100 \tag{2}$$

where C_0 depicts the initial methylene blue concentration, Ce depicts the methylene blue concentration at time t, V is the sample volume, and W is the adsorbent content (Hameed et al. 2007).

Adsorption isotherms

Adsorption isotherms are employed to determine the distribution of adsorbate molecules in the liquid phase and the adsorbent when the adsorption reaches equilibrium. Several models are available in the literature to describe the experimental adsorption isotherm data. Langmuir and Freundlich's isotherms are the most frequently employed models (Mushtaq et al. 2023).

In the Langmuir isotherm, adsorbed molecules form a single saturated layer on the surface of the adsorbent. Adsorption is directly proportional to the initial adsorbate concentration (Mushtaq et al. 2023). Equations 3 and 4 are used for the Langmuir isotherm (Naeem et al. 2017).

The linear Langmuir isotherm equation:

$$\frac{C_e}{q_e} = \frac{1}{K_L q_{max}} + \frac{C_e}{q_{max}} \tag{3}$$

where K_L is the Langmuir constant based on adsorption energy (L/g), q_{max} is the maximum adsorbing capacity of the adsorbent (constant, mg/g), Ce is the adsorbate concentration remaining in solution after adsorption (mg/L), q_e is the adsorption capacity of the adsorbent (mg/g).

Langmuir isotherm equilibrium factor (R_L):

Table 1 GC–MS conditions

Instrument	GC–MS (Shimadzu GC–MS-QP2020)	
GC conditions		
Column	Agilent HP-5MS (30 m × 0.32 mm × 0.25 μm) (length × diameter × thickness)	
Injection mode	Splitless	
Injection temperature	250 °C	
Flow control mode	Linear velocity (flow control)	
Column flow	1.2 mL min⁻¹	
Carrier gas	Helium	
Column oven temperature progress		
Rate (°C min⁻¹)	Temperature (°C)	Hold time (min)
-	40	0
4	180	0
6	300	5
MS conditions		
Ion source temp	200 °C	
Interface temp	250 °C	
Scan range	35–675 m/z	
Library	Wiley Nist	

$$R_L = \left(\frac{1}{1 + K_L C_0} \right) \tag{4}$$

Freundlich adsorption isotherm is employed in heterogeneous surfaces with multilayer adsorption. In the isotherm, the adsorbed substance amount increases initially, then the rate slows down as the solid surface is filled with gas molecules. The empirically derived Freundlich equation is expressed as follows (Mushtaq et al. 2023).

Equation 5 is used for the Freundlich isotherm.

$$\log q_e = \log K_F + \frac{1}{n} \log C_e \tag{5}$$

where; q_e is the adsorption capacity of the adsorbent (mg/g), K_F and n are experiment constants, and Ce is the adsorbate concentration remaining in solution after adsorption (mg/L).

Results

Proximate analysis of biomass samples

The results of the proximate analysis conducted on the pomegranate peel biomass and other biomass sources in the literature are presented in Table 2.

The review of the preliminary analysis results revealed that the pomegranate peel moisture and ash content were lower when compared to other biomass sources. High moisture content in biomass negatively affects conversion and fuel (Agrawalla et al. 2011; Hopa et al. 2019). High ash content increases the solid content that could not be transformed into fuel during pyrolysis ((Biswas et al. 2017). It was observed that the volatile matter content (62.2%) in pomegranate peel was lower when compared to other biomass sources. Since the volatile matter content promotes decomposition during pyrolysis, it ensures faster pyrolysis (Shadangi and Mohanty 2014). It has been determined that pomegranate peel had low lignin (10.3 wt.%) content despite high hemicellulose (57 wt.%) concentration.

TG and DTA analyses were conducted to determine the biomass's thermal behavior and pyrolysis temperatures.

The review of the thermogram plotted with TG and DTA analysis and presented in Fig. 1 demonstrated that the 10% loss of mass up to 200 °C was due to the evaporation of the moisture and volatile components at low temperatures and the sudden mass loss between 200 and 400 °C was due to the degradation of the cellulose content. Between 225 and 500 °C, where the mass loss was observed, is the pyrolysis zone and the mass loss observed in this range was around 50%. It was studied at pyrolysis temperatures in the 400–550 °C range using thermal analysis data. The endothermic peak caused by the evaporation of water is between 100 and 200 °C. The minor endothermic peak at 260–400 °C belongs to hemicellulose/cellulose, and the main endothermic peak at around 375–500 °C belongs to lignin, which is more difficult to degrade due to the aromatic groups in its structure (Hu et al. 2016; Tian et al. 2016; Song et al. 2019).
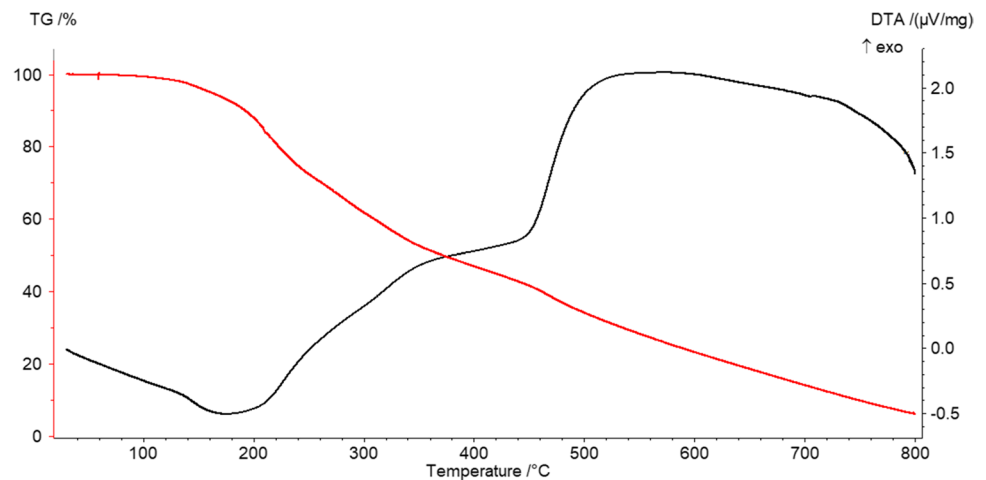
Pyrolysis results

Pyrolysis was conducted on waste pomegranate peel with particle sizes of 1.0–1.6 mm and 1.6–2.1 mm at 400 °C, 450 °C, 500 °C, and 550 °C. The liquid(bio-oil), solid, and gas product yields after pyrolysis are presented in Table 3.

The primary and secondary decomposition rates increase with the increase in temperature during pyrolysis. For this reason, liquid and gas product yields increased with pyrolysis temperature from 400 to 450 °C in both particle sizes Increasing the temperature further (500–550 °C) decreased the yields of liquid and solid products. As expected, the solid product yield was higher at low temperatures but decreased at high temperatures. With the increase in particle size, it was observed that the liquid and gas product yields improved at all temperatures, but there was no significant change in the solid product yield. It is thought that there are no significant differences between the product yields due to the closeness of the particle sizes used.

Table 2 Proximate analysis results

	Moisture (%)	Ash (%)	Volatile matter (%)	Oil (%)	Lignin (%)	Cellulose (%)	Hemicellulose (%)
Pomegranate peel (this work)	4.9	2.9	62.2	1.04	10.3	14.5	57
Tea (Rijo et al. 2021)	6.6	3.4	73.4		37.7	28.8	19.9
Fig leaf (Kar et al. 2022)	10.7	10.7	75.8		13.2	11.1	33.7
Pine cone (Brebu et al. 2010)	9.6	0.9	77.8	2.3	24.9	32.7	37.6
Sugar beet pulp (Martínez et al. 2018)	9.8	6.9	78.2		23.9	16.9	19.7
Pistachio shell (Pütün et al. 2007)	7.4	1.34	76.9	2.4	12.8	60.6	

Fig. 1 Pomegranate peel waste TG and DTA thermograms

Table 3 The results of the pyrolysis conducted under various temperatures

Pyrolysis conditions	Temperature (°C)	Liquid product (bio-oil) wt%	Solid product wt%	Gas product wt%	Water wt%
1–1.6 mm 10 °C/min	400	14.7	37.6	22.0	25.7
	450	16.0	35.1	23.1	25.8
	500	15.0	33.0	26.0	26.0
	550	14.2	31.1	30.0	26.7
1.6–2.1 mm 10 °C/min	400	13.6	37.3	28.5	20.6
	450	17.8	33.7	29.9	18.6
	500	17.3	32.1	32.3	18.4
	550	17.1	33.7	30.1	19.2

Table 4 The impact of heating rate on liquid product yield

	Heating rate (°C/min)	Liquid product (bio-oil) (wt%)	Solid product (wt%)	Gas product (wt%)	Water (wt%)
1.6–2.1 mm 450 °C	10	17.8	33.7	29.9	18.6
	18	17.1	34.1	29.1	19.7

The highest liquid (bio-oil) product yield was obtained with a particle size of 1.6–2.1 mm, 10 °C/min heating rate, and 450 °C pyrolysis temperature (17.8 wt%), which were determined as the best pyrolysis conditions. At this temperature, solid product (biochar) yield was 33.7 wt%, and gaseous product yield was 29.9 wt%.

The impact of heating rate on pyrolysis liquid product yield was investigated for the conditions that resulted in the highest liquid product yield.

As seen in Table 4, although there is no significant change in the liquid product yield, the liquid product yield with a low heating rate is slightly higher than the other. The best product yields in the liquid product are observed at low heating rates (Bridgwater et al. 2002).

Characterization of bio-oil

The bio-oil obtained using the best pyrolysis conditions was selected for characterization studies.

FT-IR analysis of bio-oil sample

FT-IR analysis was conducted to determine the functional groups in the bio-oil.

The FT-IR spectrum presented in Fig. 2 revealed that the peaks at 3150 and 3450 cm^{-1} correspond to the stretching vibration of O–H bonds. This demonstrates that it might contain phenol and alcohol components. The peak at 2928 cm^{-1} was obtained with the stretching vibration of the aliphatic C-H bond. The peak between 1680 and 1725 cm^{-1} was obtained with the carbonyl (C=O) group and originated from the ketone, aldehyde, and ester compounds in the bio-oil composition. The peak at 1607 cm^{-1} was obtained with the stretching vibration of the C=C double bond, indicating unsaturation in compound structures. The peak at 1450 cm^{-1} was the bending peak of –CH$_2$–, and the peak at 1380 cm^{-1} was the –CH$_3$ bending peak. The peaks between 700 and 800 cm^{-1} belong to the aromatic C-H bending for substituted benzene.
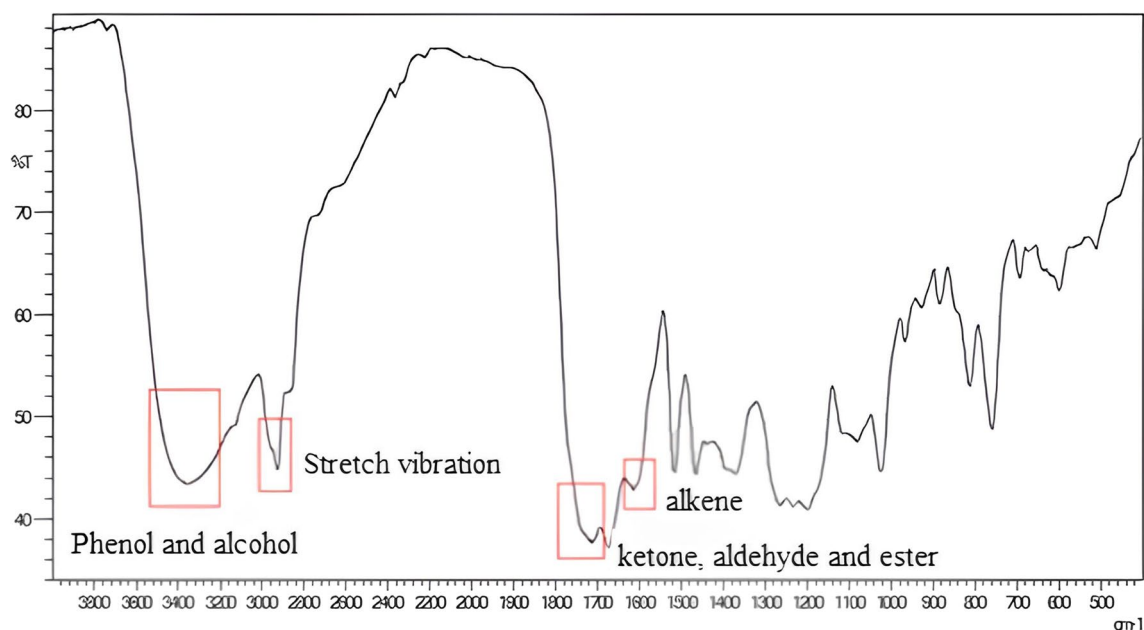
Fig. 2 FT-IR spectra of bio-oil

Calorific analysis of bio-oil sample

A calorific value analysis was conducted to determine whether the bio-oil could be employed as a fuel, and the lower calorific value was determined as 27.33 MJ/kg for the bio-oil. Compared to the lower calorific value of fuel oil (38.52 MJ/kg) (Demirel 2016), it was determined that the calorific value of bio-oil was low. It is suggested that the bio-oil should be mixed with diesel at specific rates rather than direct employment as a fuel. At the same time, the calorific value of the raw biomass was determined as 15.69 MJ/kg.

GC–MS analysis of bio-oil sample

Bio-oil obtained under the best pyrolysis conditions was selected, and GC–MS analysis was conducted to determine the bio-oil components. The 62 compounds with an accuracy rate of 80% and above and a peak area of at least 0.1% were selected among 100 components determined according to the GC–MS analysis results. These 62 components in Table 5 are classified, and the results are given in Fig. 3.

GC–MS analysis results demonstrated that phenol content was 27.9%, aldehyde content was 19.0%, acid compound content was 18.3%, ketone content was 8.7%, and aromatic compound content was 8.38%. The bio-oil had a high level of phenols. Phenolic compounds were produced from the decomposition of lignin (Patwardhan et al. 2011; Zhao et al. 2021). The ratio of aldehydes and acids in the bio-oil content was higher than the other components. These compounds, which reduce and adversely affect the

shelf life of fuels (Liang et al. 2021), can be reduced by catalytic pyrolysis with an appropriate catalyst (Zhang 2022).

Characterization of activated carbon

As a result of pyrolysis studies, the activated carbon was obtained using biochar formed under the best pyrolysis conditions. The activated carbon obtained was characterized by BET and SEM analysis.
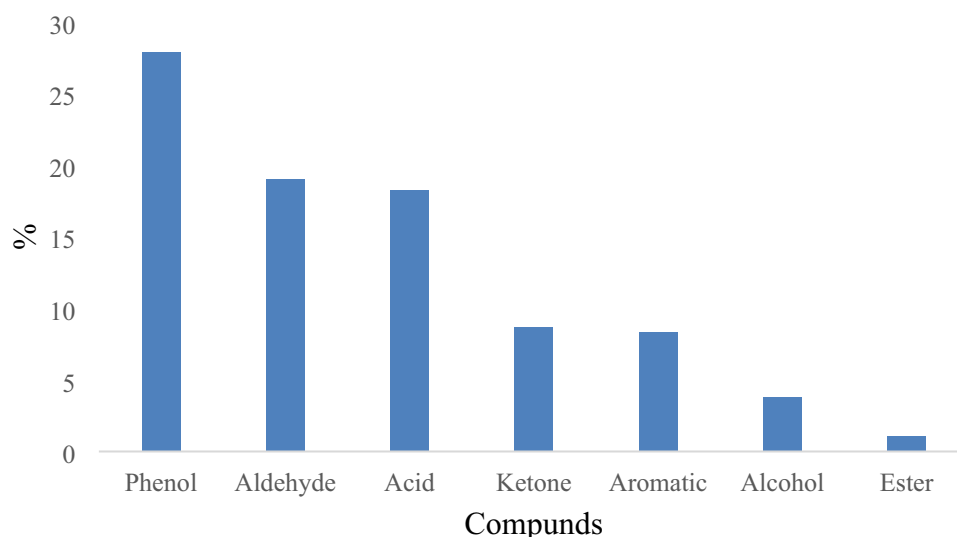
BET analysis results

The results of BET analysis to determine the surface area of activated carbon samples produced at various impregnation ratios and carbonization temperatures are given in Table 6.

The highest surface area (1307.0 m^2/g) was achieved with the carbonization conducted at 800 °C with a 3:1 impregnation ratio. It has been observed that the surface areas of activated carbons obtained at low carbonization temperatures and impregnation rates were low. The increase in the ratio of the chemical component used in the activation and the temperature allows the formation of new pores, thus increasing the micropore volume thus increasing the total surface area (Phothong et al. 2021). Activated carbon with the highest surface area was used in adsorption experiments.

Table 5 GC–MS analysis of pomegranate peel

RT min	Peak area (%)	Compound	Molecular formula	RT min	Peak area (%)	Compound	Molecular formula
57.08	0.13	9-Octadecenoic acid	$C_{18}H_{34}O_2$	19.472	0.32	Phenol, 2-ethyl-	$C_8H_{10}O$
52.848	0.27	Hexadecanoic acid	$C_{16}H_{32}O_2$	18.599	0.35	2-Cyclopenten-1-one, 3-ethyl-2-hydroxy	$C_8H_{12}O_2$
48.582	2.61	2-Furancarboxaldehyde, 5-(hydroxymethyl)-	$C_6H_6O_3$	18.34	1.83	Maltol	$C_6H_6O_3$
38.633	0.26	9H-Fluorene	$C_{13}H_{10}$	17.907	0.94	Phenol, 2,6-dimethyl-	$C_8H_{10}O$
37.854	0.19	Naphthalene, 1,6,7-tri-methyl-	$C_{13}H_{14}$	17.417	0.89	Benzofuran, 2-methyl-	C_9H_8O
36.881	0.22	5-tert-Butylpyrogallol	$C_{10}H_{14}O_3$	16.905	0.24	Benzofuran, 7-methyl-	C_9H_8O
35.951	0.2	Dibenzofuran	$C_{12}H_8O$	16.747	2.2	Phenol, 2-methoxy-	$C_7H_8O_2$
33.551	0.53	Phenol, 2-methoxy-4-(1-propenyl)-	$C_{10}H_{12}O_2$	16.502	4.08	Phenol, 3-methyl-	C_7H_8O
31.885	0.1	Naphthalene, 1,7-dime-thyl-	$C_{12}H_{12}$	15.341	2.42	Phenol, 2-methyl-	C_7H_8O
31.258	0.22	Naphthalene, 2,7-dime-thyl-	$C_{12}H_{12}$	14.368	0.58	2,3-Dimethyl-2-cyclo-penten-1-one	$C_7H_{10}O$
30.22	0.19	Biphenyl	$C_{12}H_{10}$	14.224	0.75	2-Acetyl-5-methylfuran	$C_7H_8O_2$
29.542	0.19	Phenol, 2-methoxy-4-(2-propenyl)-	$C_{10}H_{12}O_2$	14.144	0.76	2-Cyclopenten-1-one	C_5H_6O
29.391	1.07	Phenol, 2,6-dimethoxy-	$C_8H_{10}O_3$	12.256	0.39	2-Furanmethanol, acetate	$C_7H_8O_3$
27.567	0.71	5-Acetoxymethyl-2-fural-dehyde	$C_8H_8O_4$	12.133	0.12	Pentanoic acid 4-oxo	$C_5H_8O_3$
27.041	0.33	Naphthalene, 2-methyl-	$C_{11}H_{10}$	12.047	0.15	Pentanoic acid	$C_5H_{10}O_2$
26.277	0.73	Naphthalene, 1-methyl-	$C_{11}H_{10}$	11.917	3.97	Phenol	C_6H_6O
25.924	0.92	Benzeneethanol, 2-meth-oxy-	$C_9H_{12}O_2$	11.708	0.13	Benzene, 1,2,3-trimethyl-	C_9H_{12}
25.722	0.47	1,4-Benzenediol, 2,3,5-trimethyl-	$C_9H_{12}O_2$	10.713	5.47	2-Furancarboxaldehyde, 5-methyl-	$C_6H_6O_2$
25.275	0.43	1,2-Benzenediol, 3-meth-oxy-	$C_7H_8O_3$	10.591	10.25	2-Furancarboxaldehyde	$C_5H_4O_2$
22.954	4.87	1,2-Benzenediol	$C_6H_6O_2$	9.819	0.32	2,5-Furandione, dihydro-3-methylene-	$C_5H_4O_3$
22.658	0.56	3,5-Dimethyl-1H-inda-zole	$C_9H_{10}N_2$	9.668	0.25	2(3H)-Furanone, 5-methyl-	$C_5H_6O_2$
22.557	0.32	1,3-Benzodioxole, 5-ethynyl-	$C_9H_6O_2$	8.55	1.05	Butyrolactone	$C_4H_6O_2$
22.348	1.39	Phenol, 2,4,6-trimethyl-	$C_9H_{12}O$	8.32	4.07	Ethanone, 1-(2-furanyl)-	$C_6H_6O_2$
22.132	0.45	Phenol, 3,4-dimethyl-	$C_8H_{10}O$	8.096	0.66	2-Cyclopenten-1-one, 2-methyl-	C_6H_8O
21.815	0.9	Phenol, 2-methoxy-4-methyl	$C_8H_{10}O_2$	6.381	0.15	Benzene, 1,3-dimethyl-	C_8H_{10}
21.346	0.39	Phenol, 2,3-dimethyl-	$C_8H_{10}O$	6.244	0.67	2-Furanmethanol	$C_5H_6O_2$
21.00	1.41	Naphthalene	$C_{10}H_8$	5.746	0.58	2-Pentanone, 4-hydroxy-4-methyl-	$C_6H_{12}O_2$
20.892	0.62	Phenol, 4-ethyl-	$C_8H_{10}O$	4.586	0.21	3(2H)-Furanone, dihydro-2-methyl-	$C_5H_8O_2$
20.185	0.28	Ethanone, 1-(2-hydroxy-phenyl)-	$C_8H_8O_2$	3.519	1.68	Pyridine	C_5H_5N
19.926	2.46	Phenol, 2,4-dimethyl-	$C_8H_{10}O$	3.144	0.81	Propanoic acid	$C_3H_6O_2$
19.688	0.67	2,3-Dihydro-3,5-di-hydroxy-6-methyl 4H-pyran-4-one	$C_6H_8O_4$	2.235	16.8	Acetic acid	$C_2H_4O_2$

Fig. 3 The GC–MS results of the bio-oil

Table 6 BET analysis results

No	Temperature (°C)	KOH/biochar	Surface area (m²/g)	Pore volume (mL/g)
1	500	0.5:1	187.4	0.0844
2	600	0.5:1	201.4	
3	700	0.5:1	246.0	0.1121
4	800	0.5:1	610.2	0.2808
5	500	1:1	473.7	
6	600	1:1	675.6	0.3032
7	700	1:1	818.8	0.3684
8	800	1:1	978.6	0.4522
9	500	2:1	529.5	0.2426
10	600	2:1	800.4	0.3939
11	700	2:1	1161.0	0.5718
12	800	2:1	1099.0	0.6072
13	500	3:1	423.9	0.1953
14	600	3:1	871.1	0.4002
15	700	3:1	1112.0	0.5099
16	800	3:1	1307.0	0.5418

SEM analysis result

SEM analysis was conducted to determine the surface morphology of the biochar obtained with pyrolysis and the activated carbon obtained with the activation of the biochar. Activated carbon with the highest surface area was selected among the activated carbons. The review of the SEM images in Fig. 4 demonstrated that biochar activation led to a more porous structure.

It could be suggested that volatile components in the sample were removed, and pits were formed after the chemical activation conducted with KOH and the subsequent carbonization. The development of pores and the heterogeneous structure of the surface indicated that the basic structure was transformed into activated carbon (Saygılı 2017).

Adsorption results

Adsorption was tested with methylene blue (MB) dye. The effects of temperature, pH, and initial concentration parameters on adsorption were determined.

Effect of pH on MB adsorption

The effects of three pH values, 4.5, 6, and 9, were investigated on MB adsorption at 25 °C and 100 ppm initial concentration. The tests revealed that MB was removed almost completely after 30 min for all pH values. It was also determined that the adsorption rate was the highest at alkaline pH values.

As seen in Fig. 5, almost all MB content was removed after 30 min in all pH values. It was observed that the adsorption was faster at alkaline pH values. Since the adsorbent surface is covered by hydrogen at low pH, MB ions cannot be absorbed by the active regions on the adsorbent (Lai and Chen 2001). Increasing the solution pH increases the solution OH^- content, and this leads to a more negative activated carbon surface. The electrostatic attraction between MB and activated carbon surface increases, leading to an increase in MB adsorption (Pathania et al. 2017). Although the adsorption rates were higher at alkaline pH, the difference was insignificant. Thus, pH 6 was preferred in further tests.
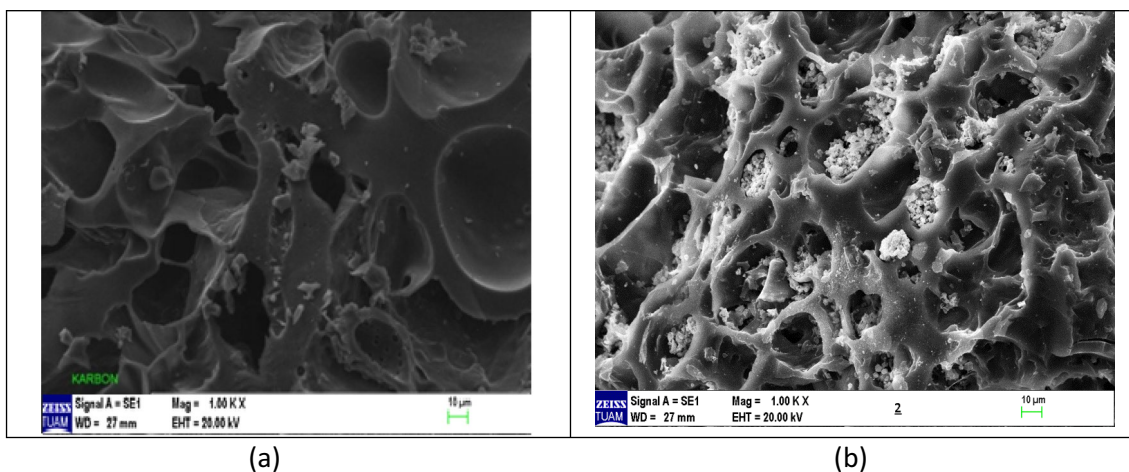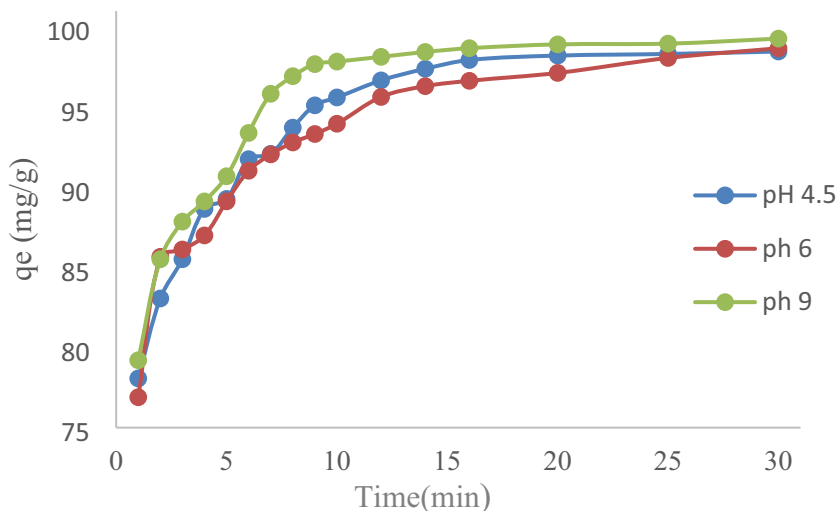
Fig. 4 SEM images. **a** Biochar. **b** Activated carbon

Fig. 5 The effect of pH on MB adsorption (100 ppm, 25 °C)

Effect of initial concentration on MB adsorption

The tests were conducted at pH 6, 25 °C, and with two concentrations (100 and 150 ppm) to determine the impact of the initial concentration on adsorption.

Figure 6 shows that adsorption rates were higher at 150 ppm. This was due to the high MB content per activated carbon unit. The increase in the initial MB concentration led to further MB adsorption per gram adsorbent since it is an essential factor for the mass transfer between the solution and the solid phase. Furthermore, when the initial concentration of dye increases, the active sites required to adsorb dye molecules are unavailable, so saturation takes place very fast (Mousavi et al. 2022).

Effect of temperature on MB adsorption

The test was conducted with 100 ppm MB solution at two temperatures (25 °C and 35 °C) and pH 6 to determine the effect of temperature on MB adsorption.

As seen in Fig. 7, the adsorption rate increased with the increase in temperature, and MB was almost completely adsorbed after 30 min. This could be due to further diffusion of the absorbed molecules with increased temperature (Ani et al. 2020).

Fig. 6 The effect of the initial concentration on MB adsorption (pH 6, 25 °C)
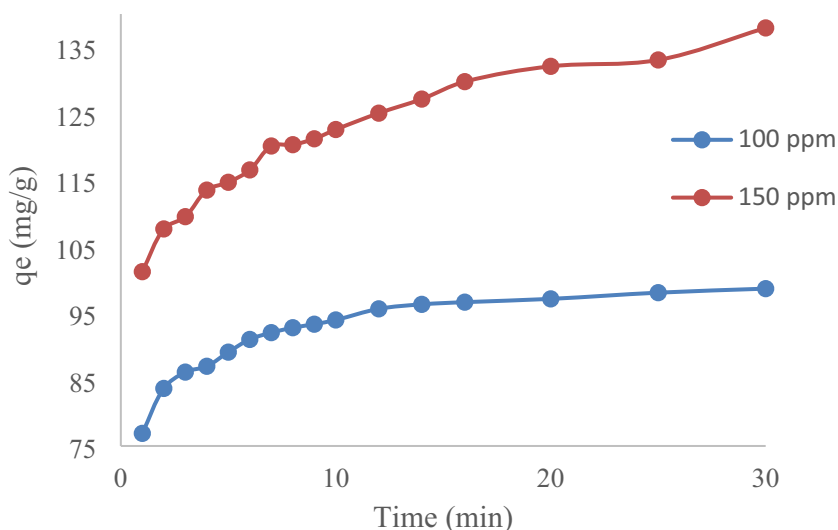
Fig. 7 The effect of temperature on MB adsorption (pH 6, 100 ppm)
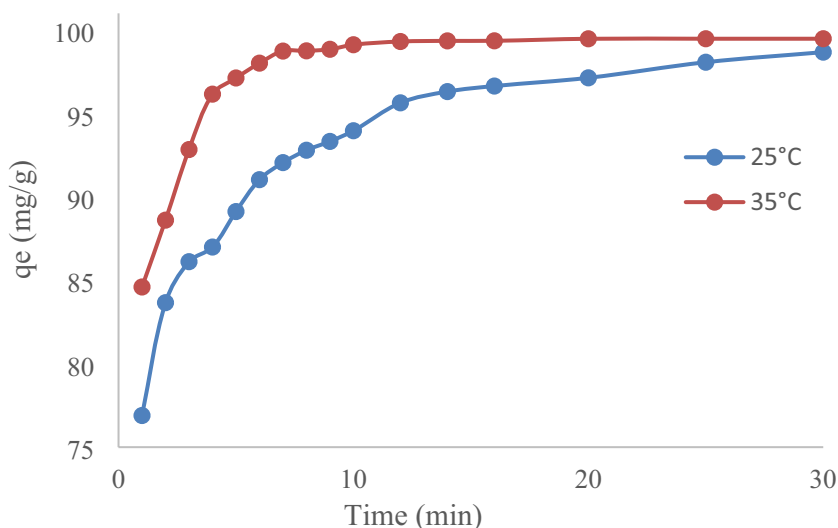
Adsorption isotherms

In the study, experimental adsorption data obtained at 25 °C and 35 °C temperatures, pH 6, and 100 ppm MB initial concentration conditions were used to create adsorption isotherms.

The Langmuir isotherm presented in Fig. 8 was plotted with the data obtained with the Langmuir equation (Eq. 3) for 100 ppm baseline concentration and pH 6.

The slope and cutoff point of the line presented in Fig. 8 were $1/q_{max}$ and $1/q_{max}K_L$, respectively. The Langmuir maximum adsorption capacity (q_{max}), Langmuir isotherm constant (K_L), correlation constant (R^2), and equilibrium factor (R_L), presented in Table 6, were calculated with the figures mentioned above. The Freundlich isotherm in

Fig. 9 was plotted with the 100-ppm baseline concentration and pH 6 data obtained with Eq. 5.

The slope and cutoff point of the line presented in Fig. 9 were $1/n$ and LnK_F, respectively. The Freundlich constants K_F and n were calculated based on the linear equation. Freundlich adsorption capacity (K_F) and correlation constant (R^2) were calculated based on these values. The resulting Langmuir and Freundlich isotherm constants are presented in Table 7.

As seen in Table 7, where Langmuir and Freundlich isotherm constants are presented, the Langmuir isotherm correlation coefficient (R^2 0.99) was higher when compared to the Freundlich isotherm correlation coefficient (R^2 0.97). Thus, MB adsorption by activated carbon was more consistent with the Langmuir model; therefore, it

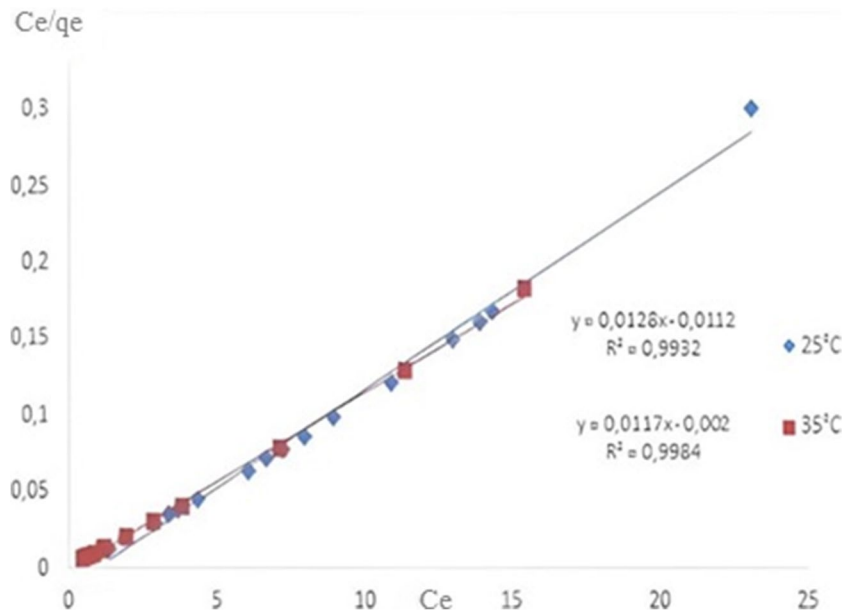**Fig. 8** Langmuir isotherm curve obtained with adsorption equilibrium data (pH 6, 100 ppm)

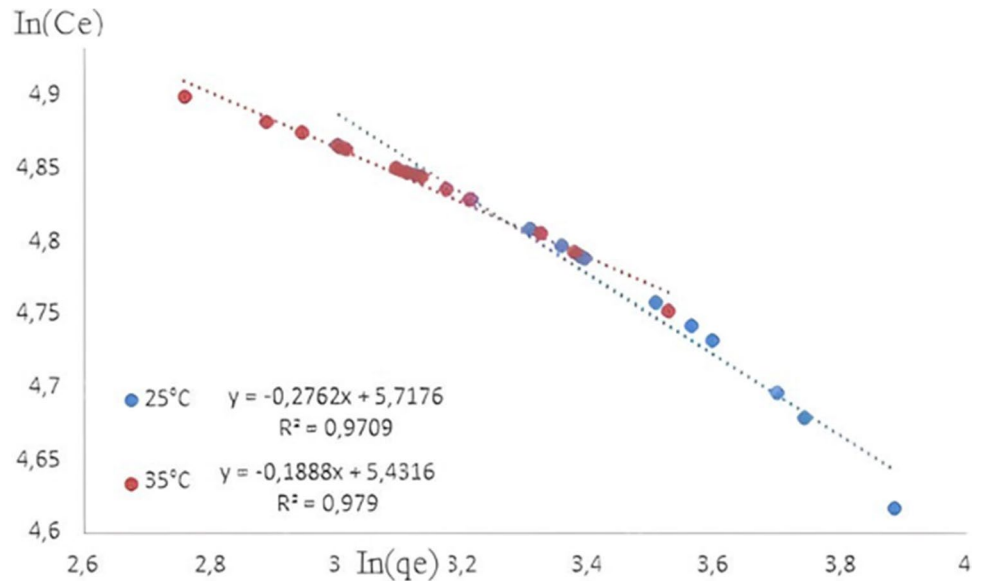**Fig. 9** Freundlich isotherm curve obtained with adsorption equilibrium data (pH 6, 100 ppm)

Table 7 Langmuir and Freundlich isotherm constants

Temperature(°C)	Langmuir constants				Freundlich constants		
	q_{max} (mg/g)	K_L (L/mg)	R_L	R^2	K_F (mg/g)	n	R^2
25	78.13	1.14	0.009	0.99	304.17	3.6	0.97
35	85.47	5.85	0.002	0.99	228.51	5.2	0.97

could be suggested that adsorption was a single layer. The dimensionless R_L constant (dissociation constant) calculated to determine the adsorption properties were between 0 and 1 at all temperatures, indicating that activated carbon was adequate for MB adsorption. Also, the high K_L, which indicated the affinity of methylene blue and activated carbon in the Langmuir isotherm, suggested that it was compatible with this isotherm (Yakout et al. 2013).

Conclusion

This study produced bio-oil and activated carbon by the pyrolysis of waste pomegranate peels. The highest bio-oil yield of 17.8 wt% was obtained at the pyrolysis temperature of 450 °C, 10 °C/min heating rate, and a 1.6–2.1 mm particle size. The caloric value of bio-oil was measured as 27.33 MJ/kg. We can say that bio-oil can be used as a fuel or mixed with fossil fuels. The major components of bio-oil were phenolic compounds by GC–MS. Due to its essential constituents, it can be utilized in many industrial applications as a chemical feedstock. Activated carbon with a surface area of 1307 m^2/g was obtained by activating biochar. The maximum adsorption capacity of MB (91 wt%) was observed at pH 9, 150 ppm initial concentration, and 35 °C temperature. The biochar obtained can be an alternative adsorbent to remove various organic and inorganic pollutants from wastewater.

Declarations

References

Agrawalla A, Kumar S, Singh R (2011) Pyrolysis of groundnut de-oiled cake and characterization of the liquid product. Bioresour Technol 102:10711–10716. https://doi.org/10.1016/j.biortech.2011.08.113

Ali L, Palamanit A, Techato K, Baloch KA, Jutidamrongphan W (2022) Valorization of rubberwood sawdust and sewage sludge by pyrolysis and co-pyrolysis using agitated bed reactor for producing biofuel or value-added products. Environ Sci Pollut Res 29:1338–1363. https://doi.org/10.1007/s11356-021-15283-6

Ani JU, Akpomie KG, Okoro UC, Aneke LE, Onukwuli OD, Ujam OT (2020) Potentials of activated carbon produced from biomass materials for sequestration of dyes, heavy metals, and crude oil components from aqueous environment. Appl Water Sci 10:1–11. https://doi.org/10.1007/s13201-020-1149-8

Ateş F, Büyüktuncer H, Yaşar B, Işık A, Biricik G, Koparal AS (2019) Comparison of non-catalytic and catalytic fast pyrolysis of pomegranate and grape marcs under vacuum and inert atmospheres. Fuel 255:115788. https://doi.org/10.1016/j.fuel.2019.115788

Biswas B, Pandey N, Bisht Y, Singh R, Kumar J, Bhaskar T (2017) Pyrolysis of agricultural biomass residues: comparative study of corn cob, wheat straw, rice straw and rice husk. Bioresour Technol 237:57–63. https://doi.org/10.1016/j.biortech.2017.02.046

Brebu M, Ucar S, Vasile C, Yanik J (2010) Co-pyrolysis of pine cone with synthetic polymers. Fuel 89(8):1911–1918. https://doi.org/10.1016/j.fuel.2010.01.029

Bridgwater A, Peacocke GVC (2000) Fast pyrolysis processes for biomass. Renew Sustain Energy Rev 4(1):1–73. https://doi.org/10.1016/S1364-0321(99)00007-6

Bridgwater A, Toft AJ, Brammer JG (2002) A techno-economic comparison of power production by biomass fast pyrolysis with gasification and combustion. Renew Sustain Energy Rev 6(3):181–246. https://doi.org/10.1016/S1364-0321(01)00010-7

Crippa M et al (2022) CO$_2$ emissions of all world countries. Publications Office of the European UnionsWeb. https://edgar.jrc.ec.europa.eu/publications. Accessed 03 October 2023

Cui C, Yang M, Zhai J, Bai W, Dai L, Liu L, Jiang S, Wang W, Ren E, Cheng C, Guo R (2023) Bamboo cellulose–derived activated carbon aerogel with controllable mesoporous structure as an effective adsorbent for tetracycline hydrochloride. Environ Sci Pollut Res 30(5):12558–12570. https://doi.org/10.1007/s11356-022-22926-9

Demirel Y (2016) Energy Sources, In: Energy. Green Energy and Technology. Springer, Cham, pp 35–71. https://doi.org/10.1007/978-3-319-29650-0_9

Dilmen H, Kaplan C, Çiftçi MC (2022) Agricultural practices of pomegranate (Punica granatum L.) producers general evaluation: the case of Siirt Province. Turkey. Turk J Agricultural Research 9(2):144–151. https://doi.org/10.19159/tutad.1049355. (In Turkish)

Hameed BH, Ahmad AL, Latiff KN (2007) Adsorption of basic dye (methylene blue) onto activated carbon prepared from rattan sawdust. Dyes Pigm 75(1):143–149. https://doi.org/10.1016/j.dyepig.2006.05.039

Hassen-Trabelsi AB, Kraiem T, Naoui S, Belayouni H (2014) Pyrolysis of waste animal fats in a fixed-bed reactor: production and characterization of bio-oil and bio-char. Waste Manage Res 34(1):210–218. https://doi.org/10.1016/j.wasman.2013.09.019

Hopa DY, Alagöz O, Yılmaz N, Dilek M, Arabacı G, Mutlu T (2019) Biomass co-pyrolysis: effects of blending three different biomasses on oil yield and quality. Waste Manage Res 37(9):925–933. https://doi.org/10.1177/0734242X19860895

Hu M, Chen Z, Wang S, Guo D, Ma C, Zhou Y, Ma S (2016) Thermogravimetric kinetics of lignocellulosic biomass slow pyrolysis using distributed activation energy model, Fraser-Suzuki deconvolution, and iso-conversional method. Energy Convers Manag 118:1–11. https://doi.org/10.1016/j.enconman.2016.03.058

İçyer NC (2012) Water extraction of phenolic components from pomegranate peel and microencapsulation of these extracts. MSc Thesis, Erciyes University (in Turkish)

Jha S, Nanda S, Acharya B, Dalai AK (2022) A review of thermochemical conversion of waste biomass to biofuels. Energies 15(17):6352. https://doi.org/10.3390/en15176352

Kar Y (2018) Pyrolysis of waste pomegranate peels for bio-oil production. Energy Sources, Part a: Recover, Utilization, Environ Eff 40:2812–2821. https://doi.org/10.1080/15567036.2018.1511652

Kar T, Keleş S, Emir Z, Kaygusuz K (2022) Fast pyrolysis of fig leaves: influence of pyrolysis parameters and characterization of bio-oil. Turk J of Anal Chem 4(2):80–87. https://doi.org/10.51435/turkjac.1143144

Lai C, Chen CY (2001) Removal of metal ions and humic acid from water by iron-coated filter media. Chemosphere 44(5):1177–1184. https://doi.org/10.1016/S0045-6535(00)00307-6

Liang J, Shan G, Sun Y (2021) Catalytic fast pyrolysis of lignocellulosic biomass: critical role of zeolite catalysts. Renew Sustain Energy Rev 139:110707. https://doi.org/10.1016/j.rser.2021.110707

Martínez CM, Cantero DA, Cocero MJ (2018) Production of saccharides from sugar beet pulp by ultrafast hydrolysis in supercritical water. J Clean Prod 204:888–895. https://doi.org/10.1016/j.jclepro.2018.09.066

Moralı U, Şensöz S (2015) Pyrolysis of hornbeam shell (Carpinus betulus L.) in a fixed bed reactor: characterization of bio-oil and biochar. Fuel 150:672–678. https://doi.org/10.1016/j.fuel.2015.02.095

Mousavi SA, Mahmoudi A, Amiri S, Darvishi P, Noori E (2022) Methylene blue removal using grape leaves waste: optimization and modeling. Appl Water Sci 12(5):112. https://doi.org/10.1007/s13201-022-01648-w

Mushtaq S, Bareen F, Tayyeb A (2023) Equilibrium kinetics and thermodynamic studies on biosorption of heavy metals by metal-resistant strains of Trichoderma isolated from tannery solid waste. Environ Sci Pollut Res 30(4):10925–10954. https://doi.org/10.1007/s11356-022-22860-w

Naeem S, Baheti V, Wiener J, Marek J (2017) Removal of methylene blue from aqueous media using activated carbon. J Text Inst 108(5):803–811. https://doi.org/10.1080/00405000.2016.1191745

Owusu PA, Asumadu-Sarkodie S (2016) A review of renewable energy sources, sustainability issues and climate change mitigation. Cogent Eng 3(1):1167990. https://doi.org/10.1080/23311916.2016.1167990

Pathania D, Sharma S, Singh P (2017) Removal of methylene blue by adsorption onto activated carbon developed from Ficus carica bast. Arab J Chem 10:S1445–S1451. https://doi.org/10.1016/j.arabjc.2013.04.021

Patwardhan PR, Brown RC, Shanks BH (2011) Understanding the fast pyrolysis of lignin. Chem Sus Chem 4(11):1629–1636. https://doi.org/10.1002/cssc.201100133

Pehlivan E, Özbay N (2018) Evaluation of bio-oils produced from pomegranate pulp catalytic pyrolysis. In: Dincer I, Çolban C, Kızılkan O (eds) Exergetic, Energetic and Environmental Dimension, 1st edn. Elsevier Science, London, pp 895–909

Phothong K, Tangsathitkulchai C, Lawtae P (2021) The analysis of pore development and formation of surface functional groups in bamboo-based activated carbon during CO_2 activation. Molecules 26(18):5641. https://doi.org/10.3390/molecules26185641

Pütün AE, Özbay N, Apaydın Varol E, Uzun BB, Ateş F (2007) Rapid and slow pyrolysis of pistachio shell: effect of pyrolysis conditions on the product yields and characterization of the liquid product. Int J Energy Res 31(5):506–514. https://doi.org/10.1002/er.1263

Rijo B, Dias APS, Ramos M, de Jesus N, Puna J (2021) Catalyzed pyrolysis of coffee and tea wastes. Energy 235:121252. https://doi.org/10.1016/j.energy.2021.121252

Saadi W, Rodríguez-Sánchez S, Ruiz B, Souissi-Najar S, Ouederni A, Fuente E (2019) Pyrolysis technologies for pomegranate (Punica granatum L.) peel wastes. Prospects in the bioenergy sector. Renew Energy 136:373–382. https://doi.org/10.1016/j.renene.2019.01.017

Saygılı H (2017) Studies on the structural, morphological and porous properties of carbonaceous material produced from a new raw material. MSc Thesis, Dicle University. (In Turkish)

Shadangi KP, Mohanty K (2014) Comparison of yield and fuel properties of thermal and catalytic Mahua seed pyrolytic oil. Fuel 117:372–380. https://doi.org/10.1016/j.fuel.2013.09.001

Siddiqui MT, Nizamuddin S, Mubarak NM, Shirin K, Aijaz M, Hussain M, Baloch HA (2019) Characterization and process optimization of biochar produced using novel biomass, waste pomegranate peel: a response surface methodology approach. Waste Biomass Valorization 10:521–532. https://doi.org/10.1007/s12649-017-0091-y

Song Y, Liu J, Evrendilek F, Kuo J, Buyukada M (2019) Combustion behaviors of Pteris vittata using thermogravimetric, kinetic, emission and optimization analyses. J Clean Prod 237:117772. https://doi.org/10.1016/j.jclepro.2019.117772

Tian L, Shen B, Xu H, Li F, Wang Y, Singh S (2016) Thermal behavior of waste tea pyrolysis by TG-FTIR analysis. Energy 103:533–542. https://doi.org/10.1016/j.energy.2016.03.022

Uçar S, Karagöz S (2009) The slow pyrolysis of pomegranate seeds: the effect of temperature on the product yields and bio-oil properties. J Anal Appl Pyrolysis 84(2):151–156. https://doi.org/10.1016/j.jaap.2009.01.005

Varma AK, Mondal P (2016) Physicochemical characterization and kinetic study of pine needle for pyrolysis process. J Therm Anal Calorim 124:487–497. https://doi.org/10.1007/s10973-015-5126-7

Yakout S, Daifullah A, El-Reefy S (2013) Adsorption of naphthalene, phenanthrene and pyrene from aqueous solution using low-cost activated carbon derived from agricultural wastes. Adsorp Sci Technol 31(4):293–302. https://doi.org/10.1260/0263-6174.31.4.293

Zhang C (2022) Review of catalytic reforming of biomass pyrolysis oil for hydrogen production. Front Chem 10:962587. https://doi.org/10.3389/fchem.2022.962587

Zhao Z, Jiang Z, Xu H, Yan K (2021) Selective production of phenol-rich bio-oil from corn straw waste by direct microwave pyrolysis without extra catalyst. Front Chem 9:700887. https://doi.org/10.3389/fchem.2021.700887

Zhong W, Li X, Luo S, Tan W, Zuo Z, Ren D (2023) The co-pyrolysis of waste urea–formaldehyde resin with pine sawdust: co-pyrolysis behavior, pyrocarbon and its adsorption performance for Cr (VI). Environ Sci Pollut Res 30(28):72854–72866. https://doi.org/10.1007/s11356-023-27297-3